

# U-HRNet: Delving into Improving Semantic Representation of High Resolution Network for Dense Prediction

Jian Wang\* Xiang Long\* Guowei Chen Zewu Wu Zeyu Chen Errui Ding  
Baidu VIS

{wangjian33, chenguowei01, wuzewu, chenzeyu01, dingerrui}@baidu.com  
lxastro0@gmail.com

## Abstract

*High resolution and advanced semantic representation are both vital for dense prediction. Empirically, low-resolution feature maps often achieve stronger semantic representation, and high-resolution feature maps generally can better identify local features such as edges, but contains weaker semantic information. Existing state-of-the-art frameworks such as HRNet has kept low-resolution and high-resolution feature maps in parallel, and repeatedly exchange the information across different resolutions. However, we believe that the lowest-resolution feature map often contains the strongest semantic information, and it is necessary to go through more layers to merge with high-resolution feature maps, while for high-resolution feature maps, the computational cost of each convolutional layer is very large, and there is no need to go through so many layers. Therefore, we designed a U-shaped High-Resolution Network (U-HRNet), which adds more stages after the feature map with strongest semantic representation and relaxes the constraint in HRNet that all resolutions need to be calculated parallel for a newly added stage. More calculations are allocated to low-resolution feature maps, which significantly improves the overall semantic representation. U-HRNet is a substitute for the HRNet backbone and can achieve significant improvement on multiple semantic segmentation and depth prediction datasets, under the exactly same training and inference setting, with almost no increasing in the amount of calculation. Code is available at PaddleSeg [47]: <https://github.com/PaddlePaddle/PaddleSeg>.*

## 1. Introduction

Dense prediction tasks, including semantic segmentation and depth estimation, among many others, are vital part of the visual understanding system. Dense prediction tasks require predicting pixel-level category labels or re-

gressing specific values, which are much more challenging than image-level prediction tasks. Keeping high resolution and strong semantic information at the same time are the key to address dense prediction tasks effectively. High resolution ensures that the final prediction granularity is as close to the pixel level as possible, and more accurate local discrimination can be obtained, such as more accurate edges. Strong semantic information ensures the overall prediction accuracy, especially for instances that are difficult to distinguish or with a relatively large area.

Deep convolutional neural networks, such as U-Net [57, 87], DeepLab [4, 5], HRNet [63, 67], which following the design of FCNs [48], have achieved exciting results in dense prediction tasks. Especially high resolution networks (HRNet) [63, 67] have achieved state-of-the-art results in dense prediction tasks, such as semantic segmentation, human pose estimation, and so on. HRNet are able to learn high resolution representations, while ensuring the transmission of semantic information between low resolution feature maps and high resolution feature maps at the same time. However, we observed that HRNet still has a lot of room for improvement. We can often see that large areas are incorrectly classified. For example, in Figure 1, the second row shows the results of HRNet. In Figure 1 (a) and (b), the entire instance is misclassified, while in (c), some blocks inside one large-area instance are misclassified. This indicates that semantic representation achieved by HRNet is still not good enough. We suppose that it could be attribute to the macro structure of HRNet, which can be summarized as two aspects below: (i) The final block from the lowest resolution branch of HRNet which has the strongest semantic representation is directly outputted without being fully propagated to higher resolution branches. (ii) The lower resolution branches of HRNet are not deep enough which makes the semantic capacity of network to be limited. While, enlarging the number of modules in the last two stages of HRNet for deeper network is obviously undesirable because of significant increasement in computation cost. U-Net [57] alleviates the above two problems to a certain extent. How-

\*Equal contribution.

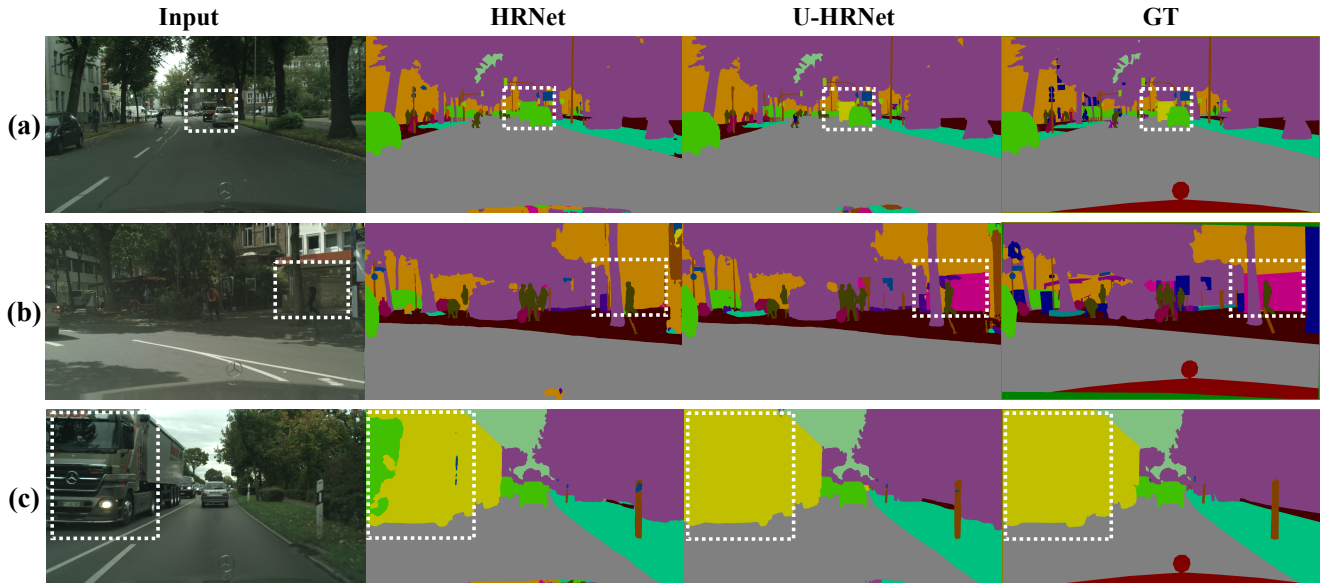


Figure 1: Semantic segmentation results of HRNet and U-HRNet. We use white dashed boxes to mark areas where the results are significantly different.

ever, in U-Net, only a single resolution is retained in each stage, and there is no fusion between different scales except merging with the residual links. We think that being able to maintain multiple scales in parallel and perform multi-scale fusion at all times is the biggest advantage of HRNet.

With the motivation of improving overall semantic representation of high resolution network without adding extra computation cost, we propose a simple and effective network named as **U-shaped High Resolution Network** (U-HRNet). It inherits the encoder-decoder structure of U-Net, which is conducive to the embedding propagation from the strongest semantic feature map to the highest resolution feature map. At the same time, it perfectly retains the advantages of HRNet, maintaining multiple scales in parallel and performing multi-scale fusion at all times. Furthermore, it reduces the number of blocks on the high-resolution branches, and reallocates their calculation to the low-resolution ones for larger semantic capacity without adding more computation. As shown in Figure 1, we can see that our U-HRNet has more advantages than HRNet in the semantic representation of difficult objects and instances with large areas. Fortunately, U-HRNet also works well together with the OCR head proposed recently by [77], as U-HRNet focuses on improving the semantic capacity of the whole network, which is not overlap with the superiority of OCR which aims to better labeling with the help of semantic relationship between objects and categories.

Thus, the contributions of this paper are following two points. 1) A simple and effective network U-HRNet is proposed, which outperforms HRNet on dense prediction tasks

with almost no increasement of computation. 2) U-HRNet together with OCR sets new state-of-the-arts on several semantic segmentation datasets.

## 2. Related work

Semantic segmentation is a pixel-level classification task, but it also requires an in-depth understanding of the semantics of the entire scene in order to assign the correct label to each pixel. Since Long *et al.* [48] proposed fully convolutional network (FCN), which includes only convolutional layers and can take an image of arbitrary size as inputs, various deep convolutional neural networks (DCNNs) have been dominate the task of semantic segmentation. To integrate more scene-level semantic context, several approaches [4, 42, 61] incorporate probabilistic graphical models into DCNNs. For example, Chen *et al.* [4] proposed to combine DCNNs with fully connected conditional random fields. Several other works, such as RefineNet [41], ExFuse [82] and CCL [11], have been proposed to capture rich contextual information from the perspective of multi-scale aggregation.

Instead of using the traditional DCNN backbones [24, 26, 31, 62, 64] commonly used in other computer vision tasks, developing a backbone network that is more suitable for segmentation can achieve better semantic segmentation performance. One popular family of DCNNs for image segmentation is based on the convolutional encoder-decoder architecture [52]. U-Net [57], and V-Net [51], are two well-known such architectures. They both need to go through multiple downsampling convolutional blocks and

then use multiple upsampling deconvolutional blocks to restore the original resolution. PSPNet [83] and Deeplabv3 series [5, 6] retain multiple spatial resolutions through different sizes of pooling kernels or dilated convolutions with different dilated rates. HRNet [63, 67] is first proposed on the human pose estimation task. It is also very suitable for semantic segmentation tasks and can achieve state-of-the-art results. HRNet directly maintains high-to-low resolution convolution streams in parallel and repeatedly exchanging the information across resolutions. Our method U-HRNet is built based on HRNet. It inherits the advantages of HRNet, keeping several resolution streams and repeating cross-resolution information transmission. At the same time, we allocate the unnecessary amount of computation on the high-resolution feature map to more meaningful parts to improve the overall semantic presentation. Our method has a certain similarity with U-Net, since they are both U-shaped networks. But different from U-Net, which only maintains a single resolution at each stage, each stage of U-HRNet will inherit one resolution stream from previous stage, which is more helpful for the fusion between different resolutions.

In addition, there are many methods based on self-attention [66] to improve the semantic representation. For example, OCNet [77] aggregates objects context by applying a self-attention module to compute the similarities of each pixel and all the other pixels. DANet [17] and Relational Context-aware Network [53] explore contextual dependencies in both spatial and channel dimensions. HC-Net [8] proposes a method to capture the dependencies between pixels within each homogeneous region and continues to model the correlation between different regions. Since our work is mainly focus on improving the backbone structure, we did not add these modules to our model for pure comparison. In fact, most of these backbone-independent improvements can be directly applied to U-HRNet to achieve better results.

Depth estimation is a pixel-level regression task, which also requires global understanding of the whole scene. Early works [59] depend on hand-crafted features to address the problem. The performance has been boosted significantly since using deep learning to predict depth maps [1, 2, 12–14, 16, 25, 32, 35, 36, 44, 45, 70, 71]. As in semantic segmentation, various backbones [5, 57, 67] have also been used in depth estimation. In this paper, we also show that U-HRNet can achieve better results in depth estimation task.

### 3. U-Shape High-Resolution Network

#### 3.1. Review of HRNet

HRNet is an excellent neural network first proposed in [63] for human pose estimation. After that, [67] further proved that HRNet could work very well on many other tasks, such as object detection, semantic segmenta-

tion. Thus it can be seen that, HRNet is strong not only at high-level semantic representation but also low-level spatial detail. As shown in Figure 2 (a), the 1/4 resolution is consistent from the beginning to the end of network, and in pace with the increasing of network of depth, more lower resolutions are added for semantic representation learning, thus improving the high-resolution representation with multi-resolution fusion.

However, HRNet may not be perfect for some dense prediction tasks. For instance, semantic segmentation is a typical dense classification task, it is important to introduce high-level global information for helping a pixel to predict its semantic category. From this point of view, we find HRNet has several drawbacks below: (i) The last block of 1/32 resolution branch which has the strongest semantic representation is directly outputted without being fully utilized. (ii) The calculation allocation among high and low resolution branches is not optimized, and the low resolution branches with strong semantic representation should be paid more attention.

#### 3.2. Architecture of U-HRNet

In order to alleviate the shortcomings mentioned above, we propose a simple and effective high resolution network named U-HRNet, which improves the semantic representation of high resolution output by restructuring the macro layout of HRNet. We will describe the details of U-HRNet from the following three perspectives: main body, fusion module and representation head.

##### 3.2.1 Main Body

Following HRNet, we input the image into a stem block decreasing the resolution to 1/4, and the main body outputs the feature map with same resolution as 1/4. Figure 2 (c) illustrates the main body of U-HRNet. Alike with U-Net, whose layout indicated in Figure 2 (b), the main body appears to be a U-Shape network in macro scope, while in micro scope, it is composed of several hr-modules proposed in [63, 67]. However, each hr-module is formed by no more than two resolution branches. This designing manner is targeted at dealing with the drawbacks of HRNet mentioned in Section 3.1. The details of restructuring are elaborated as below. Firstly, we remove high-resolution branches of the last two stages of HRNet (1/4 resolution branches of stage3 and stage4, 1/8 resolution branch of stage4), which make a lot of calculations be released. Then, for improving semantic representation of the high-resolution output, we add several stages after the lowest resolution stage. These stages gradually upsample the feature maps and merge with the features from previous stages. That makes the feature with the strongest semantic representation outputted by the lowest resolution stage can be merged with low-level high-resolution features more earlier, thus the succes-

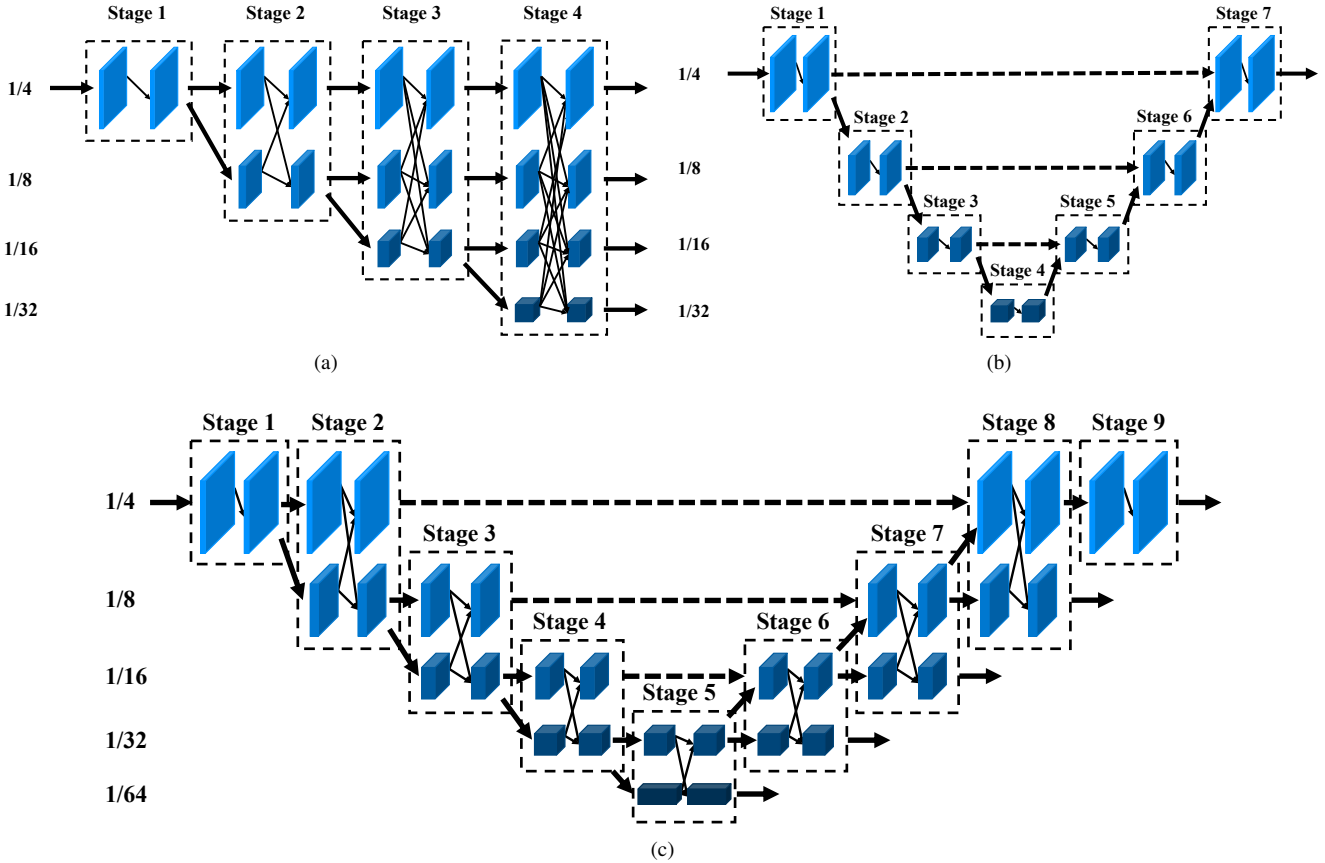


Figure 2: Illustrating the network architecture of different methods. (a) HRNet consists of parallel high-to-low resolution sub-networks with repeated hr-modules to exchange information across multi-resolution feature maps. (b) U-Net only maintains a single resolution at each stage. (c) U-HRNet is a U-shape network in macro scope. Each stage is composed of several hr-modules formed by no more than two resolution branches.

sive stages are able to infer the spatial details more precisely by analyzing the strongest representation sufficiently. Finally, we rearrange the hr-modules in different stages. We increase modules in low-resolution stages while reduce in high-resolution stages, which improving the semantic representation to a higher degree. In addition, we add a stage with 1/32 and 1/64 resolution branches for producing more informative semantic representation without need of adding extra higher resolution branches. Analogous to U-Net, several shortcuts are placed span the depth direction of network, which connect the stage2 and stage8, stage3 and stage7, stage4 and stage6 respectively. These shortcuts make the network can take advantages of both high-level features and low-level features, and meanwhile, enable the gradient to propagate directly to the previous stages.

### 3.2.2 Fusion Module

Corresponding to the shortcuts in main body, there are three fusion modules before stage8, stage7 and stage6, which

merge the low-level features outputted by the higher resolution branches of stage2, stage3 and stage4 with the up-sampled features from the higher resolution branches of stage7, stage6 and stage5 respectively. Intuitively, we can apply the method of fusion used in high resolution module for simplicity, which adding the two input features and then conducting a ReLU function for activation, as exhibited in Fusion A from Figure 3. However, we suppose that concatenating two input features can enhance the connectivity of network according to the fusion method of U-Net. Therefore, we first pool the two input features at channel dimension with a kernel size of 2 and then concatenate them among channel as the output feature, as exhibited in Fusion B from Figure 3.

### 3.2.3 Representation Head

For the representation head, we follow HRNetV2 basically. The outputted multi-resolution features are from the lower resolution branches of stage5, stage6, stage7, stage8 and

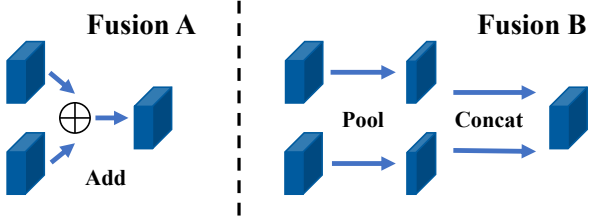


Figure 3: Fusion modules: Fusion A is the fusion module in HRNet [67], which directly adds the two input features. The proposed Fusion B first pools the two input features at channel dimension with a kernel size of 2 and then concatenates them together.

stage9. However, due to the added  $1/64$  resolution, the numbers of input channel of the convolution in the U-HRNet representation head is double to the HRNetV2. For sake of keeping a similar computation cost to the representation head of HRNetV2, we pass the multi-resolution features through a pooling operation with kernel size as 2, and then concatenate them together among the channel dimension as the input of representation head.

### 3.3. Instantiation

The main body of U-HRNet contains 9 stages with 5 resolution streams. The resolutions are  $1/4$ ,  $1/8$ ,  $1/16$ ,  $1/32$ ,  $1/64$ . The first stage contains 1 one-branch hr-module formed by 4 bottleneck residual blocks where each block has a width of 64, and is followed by one  $3 \times 3$  convolution changing the width of feature map to  $C$ , which is denoted as the width of  $1/4$  resolution stream. The 2nd to 8th stages contain 1, 5, 2, 2, 1, 1, 1 hr-modules, respectively. And all of these modules are composed by two branches, each branch in these modules consist of 4 basic residual blocks. Like the first stage, the last stage contains 1 one-branch hr-module too, while this module is formed by 4 basic residual blocks. Finally, the widths of the convolutions of the five resolution streams are  $C$ ,  $2C$ ,  $4C$ ,  $8C$  and  $16C$  respectively. The layout of U-HRNet is depicted in Figure 2 (c). Besides, for U-HRNet-small, there are two points of difference comparing to U-HRNet, which are (i) the third stage is consist of 2 hr-modules while the other stages stay same with U-HRNet, (ii) all the branches in the hr-modules from U-HRNet-small contain 2 bottleneck blocks or basic blocks.

### 3.4. Analysis

Beside the first and last stage, in U-HRNet, two-branches hr-module is mainly adopted as the basic unit for composing the network instead of the multi-resolution (two or more) parallel convolution used in HRNet and one-branch convolution sequence in U-Net. It brings several benefits which helping to improve the semantic representation. Compare to HRNet, the two-branches hr-module relaxes the limita-

tion that all resolutions need to be calculated parallel for a certain stage while without lost of the advantage of multi-resolution inference. This allows U-HRNet can attach more calculation on low resolution branches than HRNet and further improve the strongest semantic representation. Compare to U-Net, the two-branches hr-module is superior to one-branch convolution sequence on multi-scale representation learning significantly. Moreover, when stepping into next resolution, either downsampling or upsampling, U-HRNet still keeps one of the previous resolutions ongoing and fuses the features of two resolutions continuously. That makes the network can fully take advantage of the information learned before while avoiding the lost of spatial or semantic knowledge caused by changing resolution.

## 4. Semantic Segmentation

Semantic segmentation is a problem of predicting class label for each pixel in a image. It is a basic and important dense task in scene understanding. Here, we conduct extensive experiments on three popular datasets of semantic segmentation, including Cityscapes, ADE20K and LIP, and then report state-of-the-art results. In addition, we also take experiment on a medical benchmark, Synapse multi-organ CT, and then show competitive results.

### 4.1. Datasets and Evaluation Metrics

**Cityscapes.** The Cityscapes dataset [9] is a large-scale dataset used for semantic urban scene understanding. It contains 5,000 images with fine annotations and 20,000 images with coarse annotations, collected from 50 different cities. This dataset includes a total of 30 classes, 19 of which are used for actual training and validation. It is noted that in our experiments, we only use 5,000 images with fine annotations as our dataset, which is divided into 2,975, 500 and 1,525 images for training, validation and online testing. The mean IoU of all classes (mIoU) is used as the major score on this dataset, and in addition, three extra scores are reported on *test* set: IoU category(cat.), iIoU class(cla.) and iIoU category(cat.).

**ADE20K.** The ADE20k dataset [86] is a challenging scene parsing dataset which has 150 classes with 1038 image-level labels, and varies in different scenes and scales. It is splitted as training/validation/testing sets with 20K/2K/3K images included respectively. The mIoU is applied as main score on this dataset.

**LIP.** The LIP dataset [22] contains 50,462 elaborately annotated human images, in which 30,462 images are used for training, and 10,000 images are used for testing. This dataset contains 20 categories (19 human part labels and 1 background label). The mIoU is the main metric for this dataset, and pixel accuracy(acc.) and average(avg.) accuracy(acc.) are also reported.



Table 3: Semantic segmentation results on Cityscapes *test* (multi-scale and flipping). We use U-HRNet-W48, whose computation complexity is comparable to HRNetV2-W48 and dilated-ResNet-101 (D- = Dilated-) based networks, for comparison. Our results are superior in terms of the four evaluation metrics.

|   | backbone      | mIoU        | iIoU cla.   | IoU cat.    | iIoU cat.   |
|---|---------------|-------------|-------------|-------------|-------------|
| <i>Model learned on the train set</i>     |               |             |             |             |             |
| PSPNet [83]                               | D-ResNet-101  | 78.4        | 56.7        | 90.6        | 78.6        |
| PSANet [84]                               | D-ResNet-101  | 78.6        | -           | -           | -           |
| PAN [34]                                  | D-ResNet-101  | 78.6        | -           | -           | -           |
| AAF [29]                                  | D-ResNet-101  | 79.1        | -           | -           | -           |
| HRNetV2 [67]                              | HRNetV2-W48   | 80.4        | 59.2        | 91.5        | 80.8        |
| U-HRNetV2                                 | U-HRNetV2-W48 | <b>81.6</b> | <b>60.8</b> | <b>92.0</b> | <b>81.2</b> |
| <i>Model learned on the train+val set</i> |               |             |             |             |             |
| GridNet [15]                              | -             | 69.5        | 44.1        | 87.9        | 71.1        |
| LRR-4x [21]                               | -             | 69.7        | 48.0        | 88.2        | 74.7        |
| DeepLab [4]                               | D-ResNet-101  | 70.4        | 42.6        | 86.4        | 67.7        |
| LC [37]                                   | -             | 71.1        | -           | -           | -           |
| Piecewise [42]                            | VGG-16        | 71.6        | 51.7        | 87.3        | 74.1        |
| FRRN [56]                                 | -             | 71.8        | 45.5        | 88.9        | 75.1        |
| RefineNet [41]                            | ResNet-101    | 73.6        | 47.2        | 87.9        | 70.6        |
| PEARL [28]                                | D-ResNet-101  | 75.4        | 51.6        | 89.2        | 75.1        |
| DSSPN [40]                                | D-ResNet-101  | 76.6        | 56.2        | 89.6        | 77.8        |
| LKM [55]                                  | ResNet-152    | 76.9        | -           | -           | -           |
| DUC-HDC [69]                              | -             | 77.6        | 53.6        | 90.1        | 75.2        |
| SAC [80]                                  | D-ResNet-101  | 78.1        | -           | -           | -           |
| DepthSeg [30]                             | D-ResNet-101  | 78.2        | -           | -           | -           |
| ResNet38 [72]                             | WRResNet-38   | 78.4        | 59.1        | 90.9        | 78.1        |
| BiSeNet [75]                              | ResNet-101    | 78.9        | -           | -           | -           |
| DFN [76]                                  | ResNet-101    | 79.3        | -           | -           | -           |
| PSANet [84]                               | D-ResNet-101  | 80.1        | -           | -           | -           |
| PADNet [74]                               | D-ResNet-101  | 80.3        | 58.8        | 90.8        | 78.5        |
| CFNet [79]                                | D-ResNet-101  | 79.6        | -           | -           | -           |
| Auto-DeepLab [43]                         | -             | 80.4        | -           | -           | -           |
| DenseASPP [83]                            | WDenseNet-161 | 80.6        | 59.1        | 90.9        | 78.1        |
| SVCNet [10]                               | ResNet-101    | 81.0        | -           | -           | -           |
| ANNet [88]                                | D-ResNet-101  | 81.3        | -           | -           | -           |
| CCNet [27]                                | D-ResNet-101  | 81.4        | -           | -           | -           |
| DANet [17]                                | D-ResNet-101  | 81.5        | -           | -           | -           |
| SFNet [38]                                | D-ResNet-101  | 81.8        | -           | -           | -           |
| HRNetV2 [67]                              | HRNetV2-W48   | 81.6        | 61.8        | 92.1        | 82.2        |
| U-HRNet                                   | U-HRNetV-W48  | <b>82.4</b> | <b>61.9</b> | <b>92.1</b> | 82.1        |
| HRNetV2+OCR [77]                          | HRNetV2-W48   | 82.5        | 61.7        | 92.1        | 81.6        |
| U-HRNet+OCR                               | U-HRNetV-W48  | <b>82.9</b> | <b>63.1</b> | <b>92.1</b> | <b>82.4</b> |

Table 4: Semantic segmentation results on ADE20K *val* (multi-scale and flipping). (D- = Dilated-).

|                | backbone                  | mIoU         |
|----------------|---------------------------|--------------|
| PSPNet [83]    | D-ResNet-101              | 43.29        |
| PSANet [84]    | D-ResNet-101              | 43.77        |
| EncNet [78]    | D-ResNet-101              | 44.65        |
| SFNet [38]     | D-ResNet-101              | 44.67        |
| CFNet [79]     | D-ResNet-101              | 44.89        |
| CCNet [27]     | D-ResNet-101              | 45.22        |
| DANet [18]     | D-ResNet-101 + multi-grid | 45.22        |
| ANNet [88]     | D-ResNet-101              | 45.24        |
| APCNet [23]    | D-ResNet-101              | 45.38        |
| ACNet [19]     | D-ResNet-101 + multi-grid | 45.90        |
| HRNet [67]     | HRNetV2-W48               | 44.20        |
| U-HRNet        | U-HRNet-W48               | <b>46.38</b> |
| HRNet+OCR [77] | HRNetV2-W48               | 45.66        |
| U-HRNet+OCR    | U-HRNet-W48               | <b>47.75</b> |

W18-small-v2, and outperforms other small models by large margins with less calculation. (ii) U-HRNet-W48 which has similar GFLOPs as HRNetV2-W48, achieve 81.9 mIoU, 0.8 points gain over HRNetV2-W48, and also outperforms other main stream large models by large margins with much lower computation cost.

Table 5: Semantic segmentation results on LIP *val* (flipping). The overall performance of our approach is the best. (D- = Dilated-)

|                    | backbone      | extra. | pixel acc.   | avg. acc.    | mIoU         |
|--------------------|---------------|--------|--------------|--------------|--------------|
| Attention+SSL [22] | VGG16         | Pose   | 84.36        | 54.94        | 44.73        |
| DeepLabV3+ [6]     | D-ResNet-101  | -      | 84.09        | 55.62        | 44.80        |
| MMAN [49]          | D-ResNet-101  | -      | -            | -            | 46.81        |
| SS-NAN [85]        | ResNet-101    | Pose   | 87.59        | 56.03        | 47.92        |
| MuLA [54]          | Hourglass     | Pose   | <b>88.50</b> | 60.50        | 49.30        |
| JPPNet [39]        | D-ResNet-101  | Pose   | 86.39        | 62.32        | 51.37        |
| CE2P [58]          | D-ResNet-101  | Edge   | 87.37        | 63.20        | 53.10        |
| HRNetV2 [67]       | HRNetV2-W48   | N      | 88.21        | 67.43        | 55.90        |
| U-HRNet            | U-HRNetV2-W48 | N      | 88.34        | <b>67.65</b> | <b>56.66</b> |
| HRNetV2+OCR [77]   | HRNetV2-W48   | N      | 88.24        | 67.84        | 56.48        |
| U-HRNet+OCR        | U-HRNetV2-W48 | N      | 88.34        | <b>68.29</b> | <b>56.99</b> |

Table 6: Semantic segmentation results on Synapse multi-organ CT dataset. The GFLOPs is calculated on the input size 224×224. The overall performance of our approach is the best.

|               | backbone      | GFLOPs | average DSC ↑ | average HD ↓ |
|---------------|---------------|--------|---------------|--------------|
| V-Net [50]    | V-Net         | -      | 68.81         | -            |
| DARR [20]     | V-Net         | -      | 69.77         | -            |
| U-Net [57]    | ResNet-50     | -      | 74.68         | 36.87        |
| AttnUNet [60] | ResNet-50     | -      | 75.57         | 36.97        |
| TransUNet [3] | ResNet-50-ViT | 14.02  | 77.48         | 31.69        |
| U-HRNet       | U-HRNetV2-W48 | 17.01  | <b>77.49</b>  | <b>29.64</b> |

Table 3 provides the comparison of U-HRNet with state-of-the-arts methods on Cityscapes *test* set. There are two situations, learning on *train* set and learning on *train+val* set. In both situations, U-HRNet-W48 preforms better than HRNetV2-W48 and other state-of-the-arts methods.

It is worth mentioning that, U-HRNet-W48 achieves comparable mIoU with HRNetV2-W48+OCR on both *val* and *test* sets by using only 57.9%(698.6/1206.3) GFLOPs. Even more, by adding OCR module, it can further achieve 82.9 mIoU on *test* set which sets a new state-of-the-art.

**Results on the ADE20K.** Table 4 illustrates the comparison of our proposed method with state-of-the-art methods on ADE20K *val* set. U-HRNet-W48 outperforms HRNetV2-W48 by a large margin of 2.18 points, and performs better than other state-of-the-arts methods as well. Further more, U-HRNet-W48+OCR achieves 47.75 mIoU, which pushes the state-of-the-art forward significantly.

**Results on the LIP.** Table 5 shows the comparison of U-HRNet with state-of-the-art methods on LIP *val* set. U-HRNet-W48 get 0.76 points gain over HRNetV2-W48 on mIoU with a similar computation cost, and performs better than other methods as well, without using extra information, such as pose and edges. While, U-HRNet-W48+OCR achieves 56.99 mIoU which is also a new state-of-the-art.

**Results on the Synapse multi-organ CT.** As shown in Table 6, U-HRNet-W48 outperforms U-Net series networks significantly. Especially, comparing to the recent TransUNet which is transformer based, U-HRNet-W48 gets 2.05 mm improvement only with a few GFLOPs increase-ment. In addition, U-HRNet is fully convolutional with-

Table 7: Depth estimation results on NYUD-Small and NYUD-Large dataset. With our U-HRNet backbone, the performance is improved over all evaluation metrics.

| Method                 | abs-rel $\log_{10}$ rms<br>(Lower is better) |              |              | $\delta_1$ $\delta_2$ $\delta_3$<br>(Higher is better) |              |              |
|------------------------|--|--------------|--------------|--|--------------|--------------|
|                        | NYUD-Small                                   |              |              |  |              |              |
| HRNetV2-W18-small [67] | 0.186  | 0.076        | 0.591        | 0.719  | 0.933        | 0.984        |
| U-HRNet-W18-small      | <b>0.172</b>                                 | <b>0.068</b> | <b>0.534</b> | <b>0.763</b>   | <b>0.950</b> | <b>0.988</b> |
| HRNetV2-W48 [67]       | 0.156  | 0.064        | 0.510        | 0.789  | 0.957        | 0.991        |
| U-HRNet-W48            | <b>0.150</b>                                 | <b>0.061</b> | <b>0.484</b> | <b>0.811</b>   | <b>0.960</b> | 0.991        |
| NYUD-Large             |  |              |              |  |              |              |
| HRNetV2-W18-small [67] | 0.147  | 0.062        | 0.500        | 0.798  | 0.958        | 0.990        |
| U-HRNet-W18-small      | <b>0.127</b>                                 | <b>0.054</b> | <b>0.456</b> | <b>0.849</b>   | <b>0.968</b> | 0.990        |
| HRNetV2-W48 [67]       | 0.123  | 0.053        | 0.448        | 0.846  | 0.968        | 0.991        |
| U-HRNet-W48            | <b>0.117</b>                                 | <b>0.051</b> | <b>0.440</b> | <b>0.863</b>   | <b>0.970</b> | 0.991        |

out outer product operation between tensors, which is more friendly for computation than transformer based network.

## 5. Depth Estimation

Depth estimation is a problem of predicting depth value for each pixel in a image. It is a typical dense regression task in scene understanding. Here, we carry out a certain amount of experiments on a widely used dataset, NYUDv2, and exhibit competitive results.

### 5.1. Dataset

**NYUD-V2.** The NYU Depth V2 (NYUD-V2) dataset contains 120K RGB-depth pairs with a  $480 \times 640$  size, which is acquired by Microsoft Kinect from 464 different indoor scenes. Apart from the whole dataset, there are officially annotated 1449 indoor images (NYUD-Small), in which 795 images are split for training. Following previous works [33, 71], we using other 654 images as test set throughout all of the experiment of depth estimation and eigen crop is conducted. In order to verify the scalability of our method, we use a large dataset, named as NYUD-Large in this paper, for training in addition. This dataset contains 24231 RGB-depth pairs released by [33].

### 5.2. Implementation Details

**Network structures.** We apply the same network structure as used in semantic segmentation, with only the number of output channel of the last convolution adapting to depth estimation, as same as the implementation in [65].

**Training details.** The same data augmentation strategy as described in [65] is used, the RGB-depth pairs are randomly scaled with the selected ratio in 1, 1.2, 1.5 and randomly horizontally flipped. For training configuration, Adam optimizer with initial learning rate  $1e-4$  and weight decay  $1e-4$  is applied, while polynomial schedule is employed for learning rate decay. For NYUD-Small, the bath size and total number of epochs are set to 6 and 80 respectively, while 16 and 50 for NYUD-Large. Imagenet pre-training is carried out for all of the experiments.

Table 8: Compare with state-of-the-arts on NYUD. Our approach performances better than most of works except for Wei *et al.* [71] that developed a strong 3D-based method.

| Method                        | abs-rel $\log_{10}$ rms<br>(Lower is better) |              |              | $\delta_1$ $\delta_2$ $\delta_3$<br>(Higher is better) |              |       |
|-------------------------------|--|--------------|--------------|--|--------------|-------|
|                               | Eigen <i>et al.</i> [12]                     | 0.158        | -            | 0.641  | 0.769        | 0.950 |
| Chakrabarti <i>et al.</i> [2] | 0.149  | -            | 0.620        | 0.806  | 0.958        | 0.987 |
| Li <i>et al.</i> [35]         | 0.143  | 0.063        | 0.635        | 0.788  | 0.958        | 0.991 |
| Laina <i>et al.</i> [32]      | 0.127  | 0.055        | 0.573        | 0.811  | 0.953        | 0.988 |
| Fu <i>et al.</i> [16]         | 0.115  | 0.051        | 0.509        | 0.828  | 0.965        | 0.992 |
| Hu <i>et al.</i> [25]         | 0.115  | 0.050        | 0.530        | 0.866  | 0.975        | 0.993 |
| Zhang <i>et al.</i> [81]      | 0.121  | -            | 0.497        | 0.846  | 0.968        | 0.994 |
| Wang <i>et al.</i> [68]       | 0.128  | -            | 0.497        | 0.845  | 0.966        | 0.990 |
| Chen <i>et al.</i> [7]        | 0.138  | -            | 0.496        | 0.826  | 0.964        | 0.990 |
| Alhashim <i>et al.</i> [1]    | 0.123  | 0.053        | 0.465        | 0.846  | 0.974        | 0.994 |
| Wei <i>et al.</i> [71]        | <b>0.108</b>                                 | <b>0.048</b> | <b>0.416</b> | <b>0.875</b>   | <b>0.976</b> | 0.994 |
| U-HRNet-W18-small (Ours)      | 0.127  | 0.054        | 0.456        | 0.849  | 0.968        | 0.990 |
| U-HRNet-W48 (Ours)            | 0.117  | 0.051        | 0.440        | 0.863  | 0.970        | 0.991 |

## 5.3. Evaluation Metrics

Following previous methods [1, 71], we use six common metrics to evaluate the performance of monocular depth estimation quantitatively: mean absolute relative error (abs-rel), mean  $\log_{10}$  error ( $\log_{10}$ ), root mean squared error (rms), and the accuracy under threshold ( $\delta_i < 1.25^i, i = 1, 2, 3$ ).

## 5.4. Experimental Results

As shown in Table 7, both on NYUD-Small and NYUD-Large, U-HRNet outperforms HRNetV2 by a remarkable margin, in particular of the small model, which outperforms the baseline HRNetV2-W18-small at rmse by 0.057 and 0.044 on NYUD-small and NYUD-Large respectively. Meanwhile, our method is also competitive with the state-of-the-art methods on NYUDv2. As depicted in Table 8, our U-HRNet-W48 achieve a rmse of 0.440 which is better than most of the previous methods. And more impressively, U-HRNet-W18-small also get a very competitive rms of 0.456 without any other additional tricks or modules for improvement. These all indicate that our model can also work well on dense regression task.

## 6. Conclusion

In this paper, we present a U-Shape high resolution network for dense prediction tasks. It has two fundamental differences from the existing high resolution network: (i) U-HRNet adds more stages after the feature map with strongest semantic representation which enables this representation can be fully utilized for further inference. (ii) U-HRNet relaxes the constraint that all resolutions need to be calculated parallel for a newly added stage, which makes the network can assign more calculations on low-resolution stages and get stronger semantic representation. U-HRNet has been verified to be more effective on several datasets of semantic segmentation and depth estimation than the existing high resolution network with a similar computation cost, and we will explore on more other dense prediction tasks such as super-resolution, inpainting, image enhancement and so on.

## References

- [1] Ibraheem Alhashim and Peter Wonka. High quality monocular depth estimation via transfer learning. *arXiv preprint arXiv:1812.11941*, 2018. 3, 8
- [2] Ayan Chakrabarti, Jingyu Shao, and Greg Shakhnarovich. Depth from a single image by harmonizing overcomplete local network predictions. In *Advances in Neural Information Processing Systems*, pages 2658–2666, 2016. 3, 8
- [3] Jieneng Chen, Yongyi Lu, Qihang Yu, Xiangde Luo, Ehsan Adeli, Yan Wang, Le Lu, Alan L Yuille, and Yuyin Zhou. Transunet: Transformers make strong encoders for medical image segmentation. *arXiv preprint arXiv:2102.04306*, 2021. 6, 7
- [4] Liang-Chieh Chen, George Papandreou, Iasonas Kokkinos, Kevin Murphy, and Alan L. Yuille. Deeplab: Semantic image segmentation with deep convolutional nets, atrous convolution, and fully connected crfs. *IEEE Transactions on Pattern Analysis and Machine Intelligence*, 40(4):834–848, 2018. 1, 2, 7
- [5] Liang-Chieh Chen, George Papandreou, Florian Schroff, and Hartwig Adam. Rethinking atrous convolution for semantic image segmentation. *arXiv preprint arXiv:1706.05587*, 2017. 1, 3, 6
- [6] Liang-Chieh Chen, Yukun Zhu, George Papandreou, Florian Schroff, and Hartwig Adam. Encoder-decoder with atrous separable convolution for semantic image segmentation. In *European Conference on Computer Vision*, September 2018. 3, 6, 7
- [7] Yuru Chen, Haitao Zhao, and Zhengwei Hu. Attention-based context aggregation network for monocular depth estimation. *arXiv preprint arXiv:1901.10137*, 2019. 8
- [8] Yanwen Chong, Congchong Nie, Yulong Tao, Xiaoshu Chen, and Shaoming Pan. Hcnet: Hierarchical context network for semantic segmentation. *IEEE Access*, 8:179213–179223, 2020. 3
- [9] Marius Cordts, Mohamed Omran, Sebastian Ramos, Timo Rehfeld, Markus Enzweiler, Rodrigo Benenson, Uwe Franke, Stefan Roth, and Bernt Schiele. The cityscapes dataset for semantic urban scene understanding. In *IEEE Conference on Computer Vision and Pattern Recognition*, 2016. 5
- [10] Henghui Ding, Xudong Jiang, Bing Shuai, Ai Qun Liu, and Gang Wang. Semantic correlation promoted shape-variant context for segmentation. In *IEEE Conference on Computer Vision and Pattern Recognition*, June 2019. 7
- [11] Henghui Ding, Xudong Jiang, Bing Shuai, Ai Qun Liu, and Gang Wang. Context contrasted feature and gated multi-scale aggregation for scene segmentation. In *IEEE Conference on Computer Vision and Pattern Recognition*, pages 2393–2402, 2018. 2
- [12] David Eigen and Rob Fergus. Predicting depth, surface normals and semantic labels with a common multi-scale convolutional architecture. In *Proceedings of the IEEE international conference on computer vision*, pages 2650–2658, 2015. 3, 8
- [13] David Eigen, Christian Puhrsch, and Rob Fergus. Depth map prediction from a single image using a multi-scale deep network. In *Advances in Neural Information Processing Systems*, 2014. 3
- [14] Xiaohan Fei, Alex Wong, and Stefano Soatto. Geosupervised visual depth prediction. *IEEE Robotics and Automation Letters*, 4(2):1661–1668, 2019. 3
- [15] Damien Fourure, Rémi Emonet, Éliisa Fromont, Damien Muselet, Alain Trémeau, and Christian Wolf. Residual conv-deconv grid network for semantic segmentation. In *British Machine Vision Conference*, 2017. 7
- [16] Huan Fu, Mingming Gong, Chaohui Wang, Kayhan Batmanghelich, and Dacheng Tao. Deep ordinal regression network for monocular depth estimation. In *IEEE Conference on Computer Vision and Pattern Recognition*, pages 2002–2011, 2018. 3, 8
- [17] Jun Fu, Jing Liu, Haijie Tian, Yong Li, Yongjun Bao, Zhiwei Fang, and Hanqing Lu. Dual attention network for scene segmentation. In *IEEE Conference on Computer Vision and Pattern Recognition*, June 2019. 3, 7
- [18] Jun Fu, Jing Liu, Haijie Tian, Yong Li, Yongjun Bao, Zhiwei Fang, and Hanqing Lu. Dual attention network for scene segmentation. In *Proceedings of the IEEE/CVF Conference on Computer Vision and Pattern Recognition*, pages 3146–3154, 2019. 7
- [19] Jun Fu, Jing Liu, Yuhang Wang, Yong Li, Yongjun Bao, Jinhui Tang, and Hanqing Lu. Adaptive context network for scene parsing. In *Proceedings of the IEEE/CVF International Conference on Computer Vision*, pages 6748–6757, 2019. 7
- [20] Shuhao Fu, Yongyi Lu, Yan Wang, Yuyin Zhou, Wei Shen, Elliot Fishman, and Alan Yuille. Domain adaptive relational reasoning for 3d multi-organ segmentation. In *International Conference on Medical Image Computing and Computer-Assisted Intervention*, pages 656–666. Springer, 2020. 7
- [21] Golnaz Ghiasi and Charless C. Fowlkes. Laplacian pyramid reconstruction and refinement for semantic segmentation. In *European Conference on Computer Vision*, pages 519–534, 2016. 7
- [22] Ke Gong, Xiaodan Liang, Dongyu Zhang, Xiaohui Shen, and Liang Lin. Look into person: Self-supervised structure-sensitive learning and a new benchmark for human parsing. In *IEEE Conference on Computer Vision and Pattern Recognition*, pages 932–940, 2017. 5, 7
- [23] Junjun He, Zhongying Deng, Lei Zhou, Yali Wang, and Yu Qiao. Adaptive pyramid context network for semantic segmentation. In *Proceedings of the IEEE Conference on Computer Vision and Pattern Recognition*, pages 7519–7528, 2019. 7
- [24] Kaiming He, Xiangyu Zhang, Shaoqing Ren, and Jian Sun. Deep residual learning for image recognition. In *IEEE Conference on Computer Vision and Pattern Recognition*, pages 770–778, 2016. 2, 6
- [25] Junjie Hu, Mete Ozay, Yan Zhang, and Takayuki Okatani. Revisiting single image depth estimation: Toward higher resolution maps with accurate object boundaries. In *IEEE Winter Conference on Applications of Computer Vision*, pages 1043–1051. IEEE, 2019. 3, 8

- [26] Gao Huang, Zhuang Liu, Laurens Van Der Maaten, and Kilian Q Weinberger. Densely connected convolutional networks. In *IEEE Conference on Computer Vision and Pattern Recognition*, pages 4700–4708, 2017. 2
- [27] Zilong Huang, Xinggang Wang, Lichao Huang, Chang Huang, Yunchao Wei, and Wenyu Liu. Ccnet: Criss-cross attention for semantic segmentation. In *IEEE International Conference on Computer Vision*, pages 603–612, 2019. 7
- [28] Xiaojie Jin, Xin Li, Huaxin Xiao, Xiaohui Shen, Zhe Lin, Jimei Yang, Yunpeng Chen, Jian Dong, Luoqi Liu, Zequn Jie, Jiashi Feng, and Shuicheng Yan. Video scene parsing with predictive feature learning. In *IEEE International Conference on Computer Vision*, pages 5581–5589, 2017. 7
- [29] Tsung-Wei Ke, Jyh-Jing Hwang, Ziwei Liu, and Stella X. Yu. Adaptive affinity fields for semantic segmentation. In *European Conference on Computer Vision*, pages 605–621, 2018. 7
- [30] Shu Kong and Charless C. Fowlkes. Recurrent scene parsing with perspective understanding in the loop. In *IEEE Conference on Computer Vision and Pattern Recognition*, pages 956–965, 2018. 7
- [31] Alex Krizhevsky, Ilya Sutskever, and Geoffrey E Hinton. Imagenet classification with deep convolutional neural networks. *Advances in Neural Information Processing Systems*, 141(5):1097–1105, 2012. 2
- [32] Iro Laina, Christian Rupprecht, Vasileios Belagiannis, Federico Tombari, and Nassir Navab. Deeper depth prediction with fully convolutional residual networks. In *2016 Fourth international conference on 3D vision*, pages 239–248. IEEE, 2016. 3, 8
- [33] Jin Han Lee, Myung-Kyu Han, Dong Wook Ko, and Il Hong Suh. From big to small: Multi-scale local planar guidance for monocular depth estimation. *arXiv preprint arXiv:1907.10326*, 2019. 8
- [34] Hanchao Li, Pengfei Xiong, Jie An, and Lingxue Wang. Pyramid attention network for semantic segmentation. In *British Machine Vision Conference*, page 285, 2018. 7
- [35] Jun Li, Reinhard Klein, and Angela Yao. A two-streamed network for estimating fine-scaled depth maps from single rgb images. In *Proceedings of the IEEE International Conference on Computer Vision*, pages 3372–3380, 2017. 3, 8
- [36] Ruibo Li, Ke Xian, Chunhua Shen, Zhiguo Cao, Hao Lu, and Lingxiao Hang. Deep attention-based classification network for robust depth prediction. In *Asian Conference on Computer Vision*, 2018. 3
- [37] Xiaoxiao Li, Ziwei Liu, Ping Luo, Chen Change Loy, and Xiaoou Tang. Not all pixels are equal: Difficulty-aware semantic segmentation via deep layer cascade. In *IEEE Conference on Computer Vision and Pattern Recognition*, pages 6459–6468, 2017. 7
- [38] Xiangtai Li, Ansheng You, Zhen Zhu, Houlong Zhao, Maoke Yang, Kuiyuan Yang, Shaohua Tan, and Yunhai Tong. Semantic flow for fast and accurate scene parsing. In *European Conference on Computer Vision*, pages 775–793. Springer, 2020. 7
- [39] Xiaodan Liang, Ke Gong, Xiaohui Shen, and Liang Lin. Look into person: Joint body parsing & pose estimation network and a new benchmark. *IEEE Transactions on Pattern Analysis and Machine Intelligence*, 41(4):871–885, 2018. 7
- [40] Xiaodan Liang, Hongfei Zhou, and Eric Xing. Dynamic-structured semantic propagation network. In *IEEE Conference on Computer Vision and Pattern Recognition*, pages 752–761, 2018. 7
- [41] Guosheng Lin, Anton Milan, Chunhua Shen, and Ian Reid. Refinenet: Multi-path refinement networks for high-resolution semantic segmentation. In *IEEE Conference on Computer Vision and Pattern Recognition*, pages 1925–1934, 2017. 2, 7
- [42] Guosheng Lin, Chunhua Shen, Anton Van Den Hengel, and Ian Reid. Efficient piecewise training of deep structured models for semantic segmentation. In *IEEE Conference on Computer Vision and Pattern Recognition*, pages 3194–3203, 2016. 2, 7
- [43] Chenxi Liu, Liang-Chieh Chen, Florian Schroff, Hartwig Adam, Wei Hua, Alan Yuille, and Li Fei-Fei. Auto-deeplab: Hierarchical neural architecture search for semantic image segmentation. *arXiv preprint arXiv:1901.02985*, 2019. 7
- [44] Fayao Liu, Chunhua Shen, and Guosheng Lin. Deep convolutional neural fields for depth estimation from a single image. In *IEEE Conference on Computer Vision and Pattern Recognition*, 2015. 3
- [45] Fayao Liu, Chunhua Shen, Guosheng Lin, and Ian Reid. Learning depth from single monocular images using deep convolutional neural fields. *IEEE transactions on pattern analysis and machine intelligence*, 38(10):2024–2039, 2015. 3
- [46] Huijun Liu. Lightnet: Light-weight networks for semantic image segmentation, 2018. 6
- [47] Yi Liu, Lutao Chu, Guowei Chen, Zewu Wu, Zeyu Chen, Baohua Lai, and Yuying Hao. Paddleseg: A high-efficient development toolkit for image segmentation. *arXiv preprint arXiv:2101.06175*, 2021. 1
- [48] Jonathan Long, Evan Shelhamer, and Trevor Darrell. Fully convolutional networks for semantic segmentation. In *IEEE Conference on Computer Vision and Pattern Recognition*, pages 3431–3440, 2015. 1, 2
- [49] Yawei Luo, Zhedong Zheng, Liang Zheng, Tao Guan, Junqing Yu, and Yi Yang. Macro-micro adversarial network for human parsing. In *European Conference on Computer Vision*, pages 424–440, 2018. 7
- [50] F Milletari, N Navab, SAV Ahmadi, and V-net. Fully convolutional neural networks for volumetric medical image segmentation. In *Proceedings of the 2016 Fourth International Conference on 3D Vision (3DV)*, pages 565–571, 2016. 7
- [51] Fausto Milletari, Nassir Navab, and Seyed-Ahmad Ahmadi. V-net: Fully convolutional neural networks for volumetric medical image segmentation. In *2016 fourth international conference on 3D vision*, pages 565–571. IEEE, 2016. 2
- [52] Shervin Minaee, Yuri Boykov, Fatih Porikli, Antonio Plaza, Nasser Kehtarnavaz, and Demetri Terzopoulos. Image segmentation using deep learning: A survey. *arXiv preprint arXiv:2001.05566*, 2020. 2
- [53] Lichao Mou, Yuansheng Hua, and Xiao Xiang Zhu. A relation-augmented fully convolutional network for seman-

- tic segmentation in aerial scenes. In *IEEE Conference on Computer Vision and Pattern Recognition*, June 2019. 3
- [54] Xuecheng Nie, Jiashi Feng, and Shuicheng Yan. Mutual learning to adapt for joint human parsing and pose estimation. In *European Conference on Computer Vision*, pages 519–534, 2018. 7
- [55] Chao Peng, Xiangyu Zhang, Gang Yu, Guiming Luo, and Jian Sun. Large kernel matters - improve semantic segmentation by global convolutional network. In *IEEE Conference on Computer Vision and Pattern Recognition*, pages 1743–1751, 2017. 7
- [56] Tobias Pohlen, Alexander Hermans, Markus Mathias, and Bastian Leibe. Full-resolution residual networks for semantic segmentation in street scenes. In *IEEE Conference on Computer Vision and Pattern Recognition*, pages 3309–3318, 2017. 7
- [57] Olaf Ronneberger, Philipp Fischer, and Thomas Brox. U-net: Convolutional networks for biomedical image segmentation. In *International Conference on Medical image computing and computer-assisted intervention*, pages 234–241. Springer, 2015. 1, 2, 3, 7
- [58] Tao Ruan, Ting Liu, Zilong Huang, Yunchao Wei, Shikui Wei, and Yao Zhao. Devil in the details: Towards accurate single and multiple human parsing. In *AAAI Conference on Artificial Intelligence*, volume 33, pages 4814–4821, 2019. 7
- [59] Ashutosh Saxena, Min Sun, and Andrew Y Ng. Learning 3-d scene structure from a single still image. In *IEEE International Conference on Computer Vision*, pages 1–8. IEEE, 2007. 3
- [60] Jo Schlemper, Ozan Oktay, Michiel Schaap, Mattias Heinrich, Bernhard Kainz, Ben Glocker, and Daniel Rueckert. Attention gated networks: Learning to leverage salient regions in medical images. *Medical image analysis*, 53:197–207, 2019. 7
- [61] Alexander G Schwing and Raquel Urtasun. Fully connected deep structured networks. *arXiv preprint arXiv:1503.02351*, 2015. 2
- [62] Karen Simonyan and Andrew Zisserman. Very deep convolutional networks for large-scale image recognition. *arXiv preprint arXiv:1409.1556*, 2014. 2
- [63] Ke Sun, Yang Zhao, Borui Jiang, Tianheng Cheng, Bin Xiao, Dong Liu, Yadong Mu, Xinggang Wang, Wenyu Liu, and Jingdong Wang. High-resolution representations for labeling pixels and regions. *arXiv preprint arXiv:1904.04514*, 2019. 1, 3
- [64] Christian Szegedy, Wei Liu, Yangqing Jia, Pierre Sermanet, Scott Reed, Dragomir Anguelov, Dumitru Erhan, Vincent Vanhoucke, and Andrew Rabinovich. Going deeper with convolutions. In *IEEE Conference on Computer Vision and Pattern Recognition*, June 2015. 2
- [65] Simon Vandenhende, Stamatios Georgoulis, and Luc Van Gool. Mti-net: Multi-scale task interaction networks for multi-task learning. *arXiv preprint arXiv:2001.06902*, 2020. 8
- [66] Ashish Vaswani, Noam Shazeer, Niki Parmar, Jakob Uszkoreit, Llion Jones, Aidan N Gomez, Łukasz Kaiser, and Illia Polosukhin. Attention is all you need. In *Advances in Neural Information Processing Systems*, pages 5998–6008, 2017. 3
- [67] J. Wang, K. Sun, T. Cheng, B. Jiang, C. Deng, Y. Zhao, D. Liu, Y. Mu, M. Tan, X. Wang, W. Liu, and B. Xiao. Deep high-resolution representation learning for visual recognition. *IEEE Transactions on Pattern Analysis and Machine Intelligence*, pages 1–1, 2020. 1, 3, 5, 6, 7, 8
- [68] Lijun Wang, Jianming Zhang, Oliver Wang, Zhe Lin, and Huchuan Lu. Sdc-depth: Semantic divide-and-conquer network for monocular depth estimation. In *Proceedings of the IEEE/CVF Conference on Computer Vision and Pattern Recognition*, pages 541–550, 2020. 8
- [69] Panqu Wang, Pengfei Chen, Ye Yuan, Ding Liu, Zehua Huang, Xiaodi Hou, and Garrison W. Cottrell. Understanding convolution for semantic segmentation. In *IEEE Winter Conference on Applications of Computer Vision*, 2018. 7
- [70] Peng Wang, Xiaohui Shen, Zhe Lin, Scott Cohen, Brian Price, and Alan L Yuille. Towards unified depth and semantic prediction from a single image. In *Proceedings of the IEEE conference on computer vision and pattern recognition*, pages 2800–2809, 2015. 3
- [71] Yin Wei, Yifan Liu, Chunhua Shen, and Youliang Yan. Enforcing geometric constraints of virtual normal for depth prediction. *IEEE International Conference on Computer Vision*, 2019. 3, 8
- [72] Zifeng Wu, Chunhua Shen, and Anton Van Den Hengel. Wider or deeper: Revisiting the resnet model for visual recognition. *Pattern Recognition*, 90:119–133, 2019. 7
- [73] Jiafeng Xie, Bing Shuai, Jian-Fang Hu, Jingyang Lin, and Wei-Shi Zheng. Improving fast segmentation with teacher-student learning. *arXiv preprint arXiv:1810.08476*, 2018. 6
- [74] Dan Xu, Wanli Ouyang, Xiaogang Wang, and Nicu Sebe. Pad-net: Multi-tasks guided prediction-and-distillation network for simultaneous depth estimation and scene parsing. In *IEEE Conference on Computer Vision and Pattern Recognition*, pages 675–684, 2018. 7
- [75] Changqian Yu, Jingbo Wang, Chao Peng, Changxin Gao, Gang Yu, and Nong Sang. Bisenet: Bilateral segmentation network for real-time semantic segmentation. In *European Conference on Computer Vision*, pages 334–349, 2018. 7
- [76] Changqian Yu, Jingbo Wang, Chao Peng, Changxin Gao, Gang Yu, and Nong Sang. Learning a discriminative feature network for semantic segmentation. In *IEEE Conference on Computer Vision and Pattern Recognition*, pages 1857–1866, 2018. 7
- [77] Yuhui Yuan, Xilin Chen, and Jingdong Wang. Object-contextual representations for semantic segmentation. In *ECCV*, 2020. 2, 3, 6, 7
- [78] Hang Zhang, Kristin Dana, Jianping Shi, Zhongyue Zhang, Xiaogang Wang, Amrith Tyagi, and Amit Agrawal. Context encoding for semantic segmentation. In *Proceedings of the IEEE conference on Computer Vision and Pattern Recognition*, pages 7151–7160, 2018. 7
- [79] Hang Zhang, Han Zhang, Chenguang Wang, and Junyuan Xie. Co-occurrent features in semantic segmentation. In *IEEE Conference on Computer Vision and Pattern Recognition*, June 2019. 7
- [80] Rui Zhang, Sheng Tang, Yongdong Zhang, Jintao Li, and Shuicheng Yan. Scale-adaptive convolutions for scene pars-

- ing. In *IEEE International Conference on Computer Vision*, pages 2050–2058, 2017. 7
- [81] Zhenyu Zhang, Zhen Cui, Chunyan Xu, Yan Yan, Nicu Sebe, and Jian Yang. Pattern-affinitive propagation across depth, surface normal and semantic segmentation. In *Proceedings of the IEEE Conference on Computer Vision and Pattern Recognition*, pages 4106–4115, 2019. 8
- [82] Zhenli Zhang, Xiangyu Zhang, Chao Peng, Xiangyang Xue, and Jian Sun. Exfuse: Enhancing feature fusion for semantic segmentation. In *European Conference on Computer Vision*, pages 269–284, 2018. 2
- [83] Hengshuang Zhao, Jianping Shi, Xiaojuan Qi, Xiaogang Wang, and Jiaya Jia. Pyramid scene parsing network. In *IEEE Conference on Computer Vision and Pattern Recognition*, July 2017. 3, 6, 7
- [84] Hengshuang Zhao, Yi Zhang, Shu Liu, Jianping Shi, Chen Change Loy, Dahua Lin, and Jiaya Jia. Psanet: Point-wise spatial attention network for scene parsing. In *European Conference on Computer Vision*, pages 270–286, 2018. 7
- [85] Jian Zhao, Jianshu Li, Xuecheng Nie, Fang Zhao, Yunpeng Chen, Zhecan Wang, Jiashi Feng, and Shuicheng Yan. Self-supervised neural aggregation networks for human parsing. In *Workshop of IEEE Conference on Computer Vision and Pattern Recognition*, pages 1595–1603, 2017. 7
- [86] Bolei Zhou, Hang Zhao, Xavier Puig, Sanja Fidler, Adela Barriuso, and Antonio Torralba. Scene parsing through ade20k dataset. In *Proceedings of the IEEE conference on computer vision and pattern recognition*, pages 633–641, 2017. 5
- [87] Zongwei Zhou, Md Mahfuzur Rahman Siddiquee, Nima Tajbakhsh, and Jianming Liang. Unet++: A nested u-net architecture for medical image segmentation. In *Deep Learning in Medical Image Analysis and Multimodal Learning for Clinical Decision Support*, pages 3–11. Springer, 2018. 1, 6
- [88] Zhen Zhu, Mengde Xu, Song Bai, Tengting Huang, and Xiang Bai. Asymmetric non-local neural networks for semantic segmentation. In *IEEE International Conference on Computer Vision*, pages 593–602, 2019. 7